SPM to the heart: mapping of 4D continuous velocities for motion abnormality quantification

M de Craene, Nicolas Duchateau, C Tobon-Gomez, B Ghafaryasl, G Piella, K S Rhode, A Frangi

SPM TO THE HEART: MAPPING OF 4D CONTINUOUS VELOCITIES FOR MOTION ABNORMALITY QUANTIFICATION

M. De Craene[⋆†] *N. Duchateau*[⋆†] *C. Tobon-Gomez*[⋆†] *B. Ghafaryasl*[⋆†] *G. Piella*[⋆†] *K.S. Rhode*[◇] *A.F. Frangi*[⋆†‡]

CISTIB, [⋆]DTIC, Universitat Pompeu Fabra, and [†]CIBER-BBN, Barcelona, Spain.
[◇]Division of Imaging Sciences and Biomedical Engineering, KCL, UK.
[‡]Department of Mechanical Engineering, The University of Sheffield, Sheffield, UK.

ABSTRACT

This paper proposes to apply parallel transport and statistical atlas techniques to quantify 4D myocardial motion abnormalities. We take advantage of our previous work on cardiac motion, which provided a continuous spatiotemporal representation of velocities, to interpolate and reorient cardiac motion fields to an unbiased reference space. Abnormal motion is quantified using SPM analysis on the velocity fields, which includes a correction based on random field theory to compensate for the spatial smoothness of the velocity fields. This paper first introduces the imaging pipeline for constructing a continuous 4D velocity atlas. This atlas is then applied to quantify abnormal motion patterns in heart failure patients.

Index Terms— Spatiotemporal atlas, SPM, temporal registration, diffeomorphism, myocardial motion.

1. INTRODUCTION

In neuroimaging, the statistical parametric mapping methodology (SPM) [1] is a recognized paradigm for comparing anatomical information previously normalized to a common template (atlas). A SPM can be built for the comparison of scalar values (image intensities, volume changes) or multivariate parameters such as deformation tensors.

In this paper, we aim at translating SPM-based analysis to cardiology by adapting it to the analysis of myocardial motion fields. The main difference with neurology is that cardiac motion inherently includes the temporal dimension, which is usually not considered in SPM-based analysis. Additionally, SPM usually compares the displacement fields resulting from inter-subject mappings, which have no physiological meaning, in contrast to cardiac motion fields, which quantify the trajectories of material points in the heart.

The construction of a SPM usually proceeds in two steps. First, all datasets are normalized to a population atlas. Periperidis *et al.* [2] introduced the concept of spatiotemporal atlas in cardiology by separating inter-subject temporal and spatial alignment. The study presented some rendering of the obtained atlas but did not show any application of this atlas for the characterization of pathological motion.

Second, a statistical model encodes the variability of the normalized data, looking for an optimal space to represent a population and perform inter-subjects comparison. Chandrashekara *et al.* [4] proposed a PCA model for representing average cardiac motion and its variability within a population. They applied this model to reconstruct motion in new patients but not for the characterization of motion abnormalities. Suinesiaputra *et al.* [5] applied ICA to the detection of abnormal thickening in short axis slices but the analysis was limited to 2D and was not performed on all components of the vector field. Alternatively, Qian *et al.* [6] analyzed strain abnormalities by a tensor-based classification framework. However, as their method does not track material points but derives strain from Gabor filters, it does not permit the analysis of each material point of the myocardium.

In contrast, SPM techniques directly allow inter-subject comparison at each point of the built map, which corresponds in our application to each material point of the myocardium. Spatial smoothness of the input data is taken into account by introducing a convolution by a Gaussian kernel in the statistical model, and taking into account the width of this kernel in the SPM computation. As output, SPM provides a map of p-values, which grades and localizes regions where the two populations under comparison differ significantly.

The pipeline we present in this paper is an extension of Duchateau *et al.* [7] in the following directions. First, we extended the analysis to 4D sequences and quantified motion from the Time Diffeomorphic Free Form Deformation (TDFFD) algorithm [9] rather than using sequential FFD, which may cause synchronization artifacts due to the use of piecewise stationary velocities. With TDFFD, motion is represented by a 3D+t diffeomorphic transformation continuous in space and time. We modified the inter-subject normalization pipeline and included Thin-Plate Spline (TPS) transformations to obtain an accurate matching of the left ventricle

This work was supported by the Spanish Industrial and Technological Development Center (cvREMOD CEN-20091044), the Spanish Ministry of Science and Innovation, Plan E and ERDF (STIMATH TIN2009-14536-C02-01), and the European Commission's 7th Framework Program (EuHeart FP7-ICT-224495). AFF was partially funded by the ICREA-Academia program.

(LV) shape. An unbiased reference was obtained as the result of a Procrustes analysis. Finally, we improved the statistical analysis at each voxel, using a SPM-based correction taking into account its neighboring voxels, rather than doing independent voxel-wise computations that do not compensate for the smoothness of the input data. The methodology is applied to the comparison of 2 patients to a population of 15 healthy subjects, using tagged magnetic resonance imaging (t-MRI) sequences.

2. METHODS

The atlas of myocardial velocities is constructed from 15 subjects acquired using t-MRI. All details regarding protocols and enrollment criteria can be found in Tobon-Gomez *et al.* [8].

2.1. LV geometry and motion extraction

For motion and geometry quantification, we extended the pipeline described in [9]. Performing tracking backward in time from the last frame was a better choice of reference given the lack of tags in the ventricular cavities. Similarity was measured using Mean Squared Error (MSE). The metric was expressed as the sum of two terms: (1) a comparison to the first frame of the sequence, and (2) a comparison of consecutive frames.

2.2. Spatiotemporal normalization and reorientation

Spatiotemporal normalization relates any reference point X and time $T \in [0,1]$ to space x and time t coordinates of a given subject. We followed the parallel transport approach of [3] and considered a separable matching in space and time.

Spatial normalization. Spatial normalization was performed in two steps. If we consider K subjects, a set of similarity transformations $\{\phi_s^k\}_{1\leq k\leq K}$ was obtained from the original set of input shapes by Procrustes alignment. This alignment also gives an average shape that is taken as reference geometry. Bias was removed from the estimated reference by computing the average similarity transformation $\overline{A_s^k}$ and multiplying all matrices A_s^k, associated to transformations ϕ_s^k, by the inverse of this average, *i.e.*,

$$A_s^k \leftarrow A_s^k \cdot \left(\overline{A_s^k}\right)^{-1}.$$

This ensures the average of all similarity transforms to be equal to identity. The same $\overline{A_s^k}$ is also applied to the average Procrustes mesh to get the unbiased reference.

All meshes are then aligned to the unbiased mesh by a set $\{\phi_p^k\}$ of Thin Plate Spline (TPS) transformations. Source and target landmarks were chosen after consistent decimation of the two input meshes according to the subsampling strategy described in Hoogendoorn *et al.* [10].

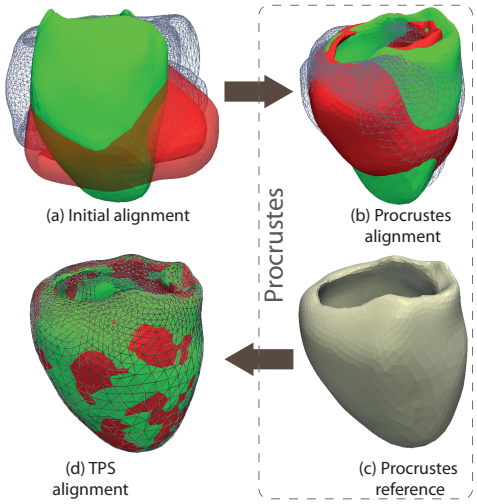

Fig. 1: Spatial normalization consists of two steps. First, the initial set of shapes is aligned (a) using similarity transformations (b) and a reference shape is computed using Procrustes' method (c). Then, the alignment of each shape to the reference is refined using a TPS transformation (d).

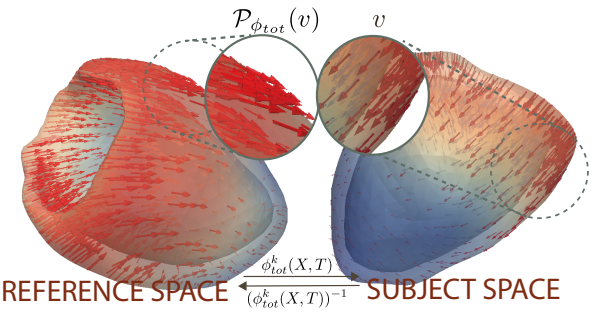

Fig. 2: Local reorientation of the velocity field attached to the LV shape.

From the unbiased mesh, the total spatial normalization mapping to reach each subject is then

$$\phi_{ps}^k(X) = \phi_p^k \circ \phi_s^k(X) \tag{1}$$

Temporal normalization. For temporal normalization, we followed an approach similar to [2]. Instead of working on intracavity volume curves, we chose to manually detect feature points in the averaged longitudinal strain curves (see Fig. 3). All temporal landmarks were normalized by the number of frames in the sequence and then averaged over all atlas subjects to produce a set of normalized landmarks. A piecewise linear interpolation was then used to match subject to normalized landmarks.

Reorientation. If $\phi_m^k(x,t)$ stands for the diffeomorphic motion computed by TDFFD [9] from a velocity field $v^k(x,t)$,

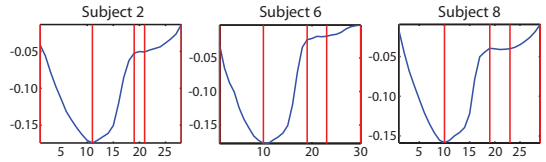

Fig. 3: Temporal landmarks manually defined for 3 subjects from the longitudinal strain curve averaged over all segments.

velocity can be reoriented at any (X, T) using

$$\mathcal{P}_{\phi_{tot}}(v^k)(X,T) = D(\phi^k_{ps})^{-1}(\cdot)\Big|_{\phi^k_{ps}(X)} \cdot (v^k \circ \phi^k_{tot}(X,T)) \tag{2}$$

where

$$\phi^k_{tot}(X,T) = \phi^k_m(\phi^k_{ps}(X), \phi^k_t(T)) \quad , \tag{3}$$

D is the local orientation/scaling matrix extracted from the inter-subject mapping and ϕ^k_t is the temporal mapping described in the former paragraph. The reorientation process is illustrated in Fig. 2.

2.3. Statistics

Hotelling's T-square statistic is computed from the reoriented velocity vectors $\nu^k = \mathcal{P}_{\phi_{tot}}(v^k)(X,T)$ according to

$$\tau^2 = \alpha(\nu^k - \overline{\nu^k})^t \cdot \Sigma^{-1} \cdot (\nu^k - \overline{\nu^k}) \tag{4}$$

where $\alpha = K/(K+1)$, $\overline{\nu^k}$ and Σ are the velocity average and covariance defined as in [7]. The spatiotemporal resolution of the velocity field is inherently related to the width of the kernel used to represent it in the TDFFD [9] registration framework. If we take as full-width at half-maximum ($FWMH_d$) the spacing between control points in the d direction (here defined as w_d), the number of resolution elements (resels) [1] in the velocity spatiotemporal domain is then

$$R = V/(w_x \cdot w_y \cdot w_z \cdot w_t) \quad , \tag{5}$$

where V is the volume of the bounding box of the normalized geometry computed in Sec. 2. Note that the control points gird is sparse in space, but not in time since we place one control point at every frame. Thus, spatial and temporal resolutions are handled differently. The detection and quantification of motion abnormalities requires to compute the p-value of observing a τ_{max} value in the myocardial domain exceeding a given threshold τ. Worsley *et al.* [1] proved that this p-value can be approximated by the Euler characteristic:

$$p(\tau_{max} > \tau) \approx \epsilon = (4\log_e(2))^{\frac{3}{2}} R\,(2\pi)^{-2}(\tau^2 - 1)e^{-\frac{1}{2}\tau^2} \quad . \tag{6}$$

This approximation is valid if the original velocity distribution (before smoothing) can be approximated by a Gaussian distribution and if the search volume V is large relative to the smoothness of the image [1].

3. RESULTS

Fig. 3 shows in three subjects the temporal landmarks used for normalizing myocardial dynamics of the atlas population. The impact of this temporal alignment is illustrated in Fig. 4 for all subjects by showing velocity curves before (a) and after (b) alignment in AHA segment # 6. Velocity curves in this segment can then be averaged to compute the average velocity profile in the atlas (bold curve in Fig. 6). Similarly, longitudinal average velocity curves are plotted for all segments in Fig. 6, the color of each curve corresponds the legend in the Bull's eye diagram.

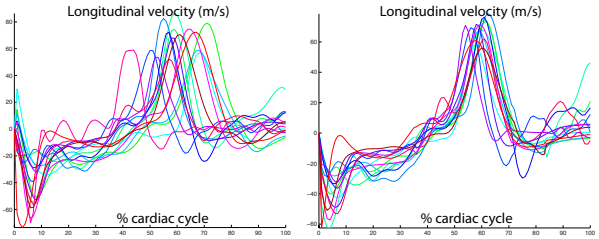

(a) Without temporal normalization (b) With temporal normalization

Fig. 4: Impact of temporal normalization shown for all subjects in one basal anterolateral AHA segment (#6, see bold curve in Fig. 6).

We then computed the Euler characteristic from (6) for one healthy subject (after leave-one-out) and for two patients suffering from dyssynchrony. The ϵ value obtained at 33% of the cardiac cycle (end of systole) is plotted using a color scale in the top part of Fig. 5. The temporal evolution of ϵ averaged over space in two AHA segments (#3 and #8) is plotted in the bottom part of Fig. 5.

In both patients, abnormality peaks were observed at the end of systole. Since both patients present assynchronous motion, the average strain curve only provides the end-systolic time for the whole LV. Around this average end-systolic time, segments contracting too late or relaxing too early trigger velocity sign difference with respect to the healthy population, hence generating high p-values of abnormality. In Patient #2, incorrect ECG triggering during the MR acquisition warped the end of the diastolic phase at time 0. This induced the first abnormality peak in this patient. Finally, for a healthy case the left ventricle has a reduced motion at end diastole. For the two patients, the abnormality peaks casted at end of diastole raised from late ventricular filling.

4. DISCUSSION AND CONCLUSIONS

This paper introduced a novel pipeline for spatiotemporal normalization of motion fields. By transporting 3D+t myocardial velocity fields to the same spatiotemporal system of coordinates, SPM-based concepts can be translated to the field of cardiology for quantifying abnormal motion patterns. With

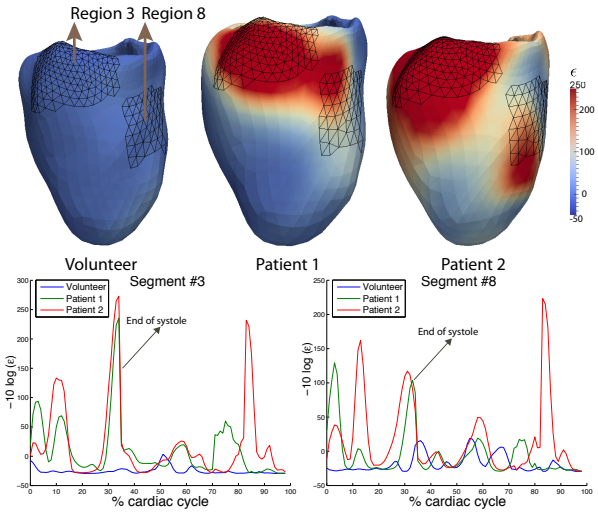

Fig. 5: (Top) p-value as approximated by the Euler characteristic plotted as color map at $t = 33\%$ cardiac cycle, and (Bottom) as a function of time, averaged over space in two AHA segments (#3 and #8).

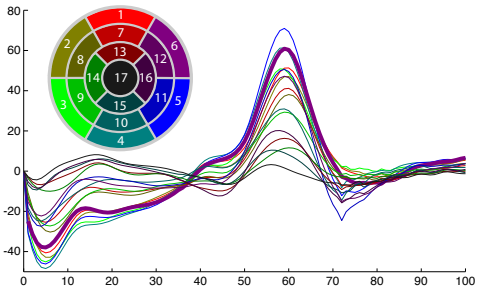

Fig. 6: Mean velocity curves in all 17 AHA regions. An example of the variability over subjects can be seen from Fig. 4 in segment # 6.

respect to our earlier work [7], we extended it to 4D sequences and used TDFFD [9] tracking. We modified the spatiotemporal normalization procedure by including TPS transformations. Finally, we modified the statistical tests by applying SPM p-value computations to 4D reoriented velocity fields. The novelty of this paper does not reside in each individual component but in their combination for statistically modeling cardiac velocity fields. Our aim is to encourage SPM experts to translate their technologies to the cardiac imaging community. The temporal normalization scheme presented in this paper reduced the dispersion in the velocity traces and aligned the main systolic and diastolic peaks. However, some variability was still observed in secondary peaks. Improving temporal normalization is expected to reduce this unnecessary variability and improve the accuracy of abnormality quantification. Future work will compare our quantification of pathological motion to visual scoring by clinicians. We also will extend our pipeline to handle the strain tensor, which is known to be more sensitive to characterize abnormalities of the cardiac function resulting from ischemia or fibrosis.

5. REFERENCES

[1] K. J. Worsley, M. Andermann, T. Koulis, D. MacDonald, and A. C. Evans, "Detecting changes in nonisotropic images," *Human brain mapping*, vol. 8, no. 2-3, pp. 98–101, Jan. 1999.

[2] D. Perperidis, R. H. Mohiaddin, and D. Rueckert, "Spatio-temporal free-form registration of cardiac MR image sequences.," *Med. Image Analysis*, vol. 9, no. 5, pp. 441–56, Oct. 2005.

[3] A. Qiu, M. Albert, L. Younes and M.I. Miller. "Time sequence diffeomorphic metric mapping and parallel transport track time-dependent shape changes," *Neuroimage*, 45(1 S1):S51–60, 2009.

[4] R. Chandrashekara, A. Rao, G. I. Sanchez-Ortiz, R. H. Mohiaddin, and D. Rueckert, "Construction of a statistical model for cardiac motion analysis using nonrigid image registration," in *Proc. IPMI*, vol. 18, pp. 599–610, 2003.

[5] A. Suinesiaputra, A. F. Frangi, T. Kaandorp, H. J. Lamb, J. J. Bax, J. Reiber, and B. Lelieveldt, "Automated detection of regional wall motion abnormalities based on a statistical model applied to multislice short-axis cardiac MR images," *IEEE Trans. on Med. Imaging*, vol. 28, no. 4, pp. 595–607, 2009.

[6] Z. Qian, Q. Liu, D. Metaxas, and L. Axel, "Identifying Regional Cardiac Abnormalities from Myocardial Strains Using Non-Tracking-Based Strain Estimation and Spatio-Temporal Tensor Analysis," *IEEE Trans. on Med. Imaging*, vol. 30, no. 12, pp. 2017–29, 2011.

[7] N. Duchateau, M. De Craene, G. Piella, E. Silva, A. Doltra, M. Sitges, B.H. Bijnens, and A.F. Frangi, "A spatiotemporal statistical atlas of motion for the quantification of abnormal myocardial tissue velocities," *Med. Image Analysis*, vol. 15, no. 3, pp. 316–28, 2011.

[8] C. Tobon-Gomez, M. De Craene, A. Dahl, S. Kapetanakis, G. Carr-White, A. Lutz, V. Rasche, P. Etyngier, T. Schaeffter, C. Riccobene, Y. Martelli, O. Camara, A.F Frangi, and K.S. Rhode, "A multimodal database for the 1st Cardiac Motion Analysis Challenge," in *Proc. STACOM, LNCS*, (In press) 2011.

[9] M. De Craene, G. Piella, O. Camara, N. Duchateau, E. Silva, A. Doltra, J. D'hooge, J. Brugada, M. Sitges, A.F. Frangi, "Temporal Diffeomorphic Free-Form Deformation: Application to Motion and Strain Estimation from 3D Echocardiography," *Med. Image Analysis*, vol. 16, no. 2, pp. 427–50, 2012.

[10] C. Hoogendoorn, A. Pashaei, R. Sebastian, F. Sukno, O. Cámara, and A.F. Frangi, "Sensitivity Analysis of Mesh Warping and Subsampling Strategies for Generating Large Scale Electrophysiological Simulation Data," *Proc. FIMH*, pp. 418–26, 2011.